

Distributed sensing based real-time process monitoring of shape memory polymer components

Madhubhashitha Herath^{1,2}  | Chris Emmanuel^{1,3} | Janitha Jeewantha^{1,3} | Jayantha Epaarachchi^{1,3} | Jinsong Leng⁴

¹Centre for Future Materials, University of Southern Queensland, Toowoomba, Queensland, Australia

²Department of Engineering Technology, Faculty of Technological Studies, Uva Wellassa University, Badulla, Sri Lanka

³School of Mechanical and Electrical Engineering, Faculty of Health Engineering and Sciences, University of Southern Queensland, Toowoomba, Queensland, Australia

⁴Center for Composite Materials and Structures, Harbin Institute of Technology, Harbin, China

Correspondence

Madhubhashitha Herath, Department of Engineering Technology, Faculty of Technological Studies, Uva Wellassa University, Badulla, Sri Lanka.
Email: madhubhashitha@uwu.ac.lk

Abstract

Shape memory polymer (SMP) materials have the capacity to undergo large deformations imposed by mechanical loading, hold a temporary shape, and then recover their original shape upon exposure to a particular external stimulus. The fiber reinforced shape memory polymer composites (SMPCs) with enhanced structural performances give a boost to breakthrough technologies for large-scale engineering applications. This article presents a novel technique for distributed optical fiber sensor (DOFS) embedded SMPCs intended for real-time process monitoring of large-scale engineering applications such as deployable space structures. Herein a carbon fiber reinforced SMPC was tested under a three-point flexural shape memory process and the DOFS data were acquired through optical backscatter reflectometry. Experiments were conducted in a temperature controlled thermal chamber coupled with a 10 kN electromechanical testing system. DOFSs offered unique advantages for spatially distributed dynamic temperature and strain measurements during the shape memory process. Compared to the standard test method dynamic mechanical analysis, larger samples can be tested effectively by using a single DOFS with large strain levels and shape complexity. The proposed technique demonstrated the ability of embedded DOFSs for in-situ shape memory characterization such as shape fixity ratio, shape recovery ratio and recovery rate. This technique will eliminate the challenges hindering the process monitoring and performance evaluation of large SMPC components operating in their real working environments.

KEYWORDS

applications, characterization, composites, stimuli-sensitive polymers, viscoelasticity

1 | INTRODUCTION

Shape memory polymers (SMPs) and their composites (SMPCs) are smart materials that are capable of switching between a temporary and an original shape. The temporary shape is meta-stable and a rapid deformation is triggered by an external stimulus until it recovers

to a more stable state.¹ Various stimulus methods, such as electro-activated, light-responsive, magnetic field activated, chemically activated, microwave activated and water-induced have been established to date.² Because of their unique advantages of high shape deformability, large recoverability, manufacturability, biodegradability, and tailorable glass transition temperature, global research

interest in these materials has been rapidly growing.³ Moreover, the recent advances in engineered nanoparticles facilitated advanced functional polymer composites.^{4–6} SMPs and SMPCs have a wide range of applications, from micro-scale to large-scale engineering. These intelligent smart materials have been extensively studied for biomedical, textile, aerospace, civil infrastructure and structural engineering applications to date.^{7–11}

By applying an external load at a temperature higher than the glass transition temperature (T_g), a thermally induced SMP material is programmed to the desired shape. The material is then cooled until it turns into a frozen polymer at a low temperature, while the programmed shape remains fixed. Afterwards, the applied load is removed. As a result, the strain decreases slightly and the material takes on the fixed shape. In the last step, the temperature is increased over T_g . Consequently, the strain relaxes and the material returns to the initial shape.¹² This process is called the stress-free strain recovery cycle of an SMP material. Moreover, researchers have studied the constrained strain stress recovery characteristics of SMP materials.^{13,14}

Recent advancements in SMP and SMPCs have enabled reversible and multiple shape memory behaviors.¹ Glass fiber reinforced (GFR) and carbon fiber reinforced (CFR) SMPCs with enhanced structural performances and recovery forces have been developed over the last few decades to meet the sophisticated demands of large-scale engineering applications that were previously hindered for several years.⁸ SMPC materials with superior structural performances can be potential candidates for space deployable structures, aerospace expansion structures, morphing structures and locking-release structures.^{8,15}

Analytical studies on the viscoelastic, thermomechanical, and shape memory behaviors of SMPCs are crucial to develop precise and reliable engineering applications. Conventionally the thermomechanical characteristics of SMPCs are quantified by the dynamic mechanical analysis (DMA).¹⁶ DMA experiments are capable of quantifying the crucial properties such as glass transition temperature, storage modulus, shape fixity ratio, shape recovery ratio and shape recovery rate. The DMA experiments are generally conducted during the material design and development phases. According to the ASTM D5418 testing standard, the DMA flexural test (dual cantilever) method provides a simple means of characterizing the thermomechanical behavior of plastic compositions using a very small amount of material.¹⁷ Since small specimen geometries are examined, it is essential that the specimens be representative of the material being tested. The data collected can be employed for quality assurance and research and development. The fundamental inadequacy of DMA is that the test specimens are small rectangular shapes (approximately $60 \times 15 \times 5 \text{ mm}^3$).^{14,17,18}

In addition, the recovery angles of SMP components during their shape recovery phase have been generally measured by compass tools.¹⁹ The coordinate measuring machines (CMM) and video-based image processing techniques have been employed to examine the shape fixity and shape recovery behaviors of SMPC structural components.^{14,20} Furthermore, the digital image correlation (DIC) technique is able to monitor the strain changes in SMPCs during their thermomechanical cycles.²¹ Thermal imaging cameras and thermocouples have been used to investigate the heat distribution inside SMPCs during the shape memory process.^{20,22} Moreover, surface-mounted fiber Bragg grating (FBG) sensors have the ability to measure temperature and strain variations for a short distance (approximately 1 cm) on an SMPC.^{23,24} Thus far only a few prototype SMPC applications have been monitored during their shape memory process at the actual operational environment.^{25–27} The performance evaluation and process monitoring techniques currently used for large SMPC components are given in Table 1. The major limitation of these existing methods is that the simultaneous measuring of multiple locations over a SMPC component that are subjected to concurrent shape memory processes.

This article proposes a distributed optical fiber sensor (DOFS) based real-time process monitoring technique for large-scale SMPC components. In comparison to the existing SMPC characterization and performance evaluation techniques, the distributed optical fiber sensors provide distinct advantages for spatially distributed strain and temperature measurements over long distances of hundreds of kilometers.^{28,29} As a result, the embedded DOFSs can be used to measure dynamic strains as well as varying temperatures across large areas of SMPC components. At present, optical fiber sensors are widely used to monitor the structural health of reinforced composite structures.²⁸ Interestingly, fiber optic sensors can be strategically embedded into fiber reinforced SMPC components during their manufacturing process.^{30–32} Our previous studies revealed the ability of embedded optical fibers to send light energy into the SMPC materials for light activation,³⁰ analyze the curing kinetics of SMPCs,³³ and evaluate in-situ shape memory performances of SMPCs.³² The state-of-the-art technique presented in this article can be used to monitor the real-time shape memory behavior of large-scale SMPC components such as deployable space habitats and solar panel arrays operating in their real working environment. Herein dynamic temperature and strain profiles during the full shape memory cycles of a CFR SMPC were measured by means of DOFSs. Based on the obtained measurements, real-time heat distribution throughout the SMPC component and geometric shape changes of the SMPC component

TABLE 1 Existing performance evaluation techniques for large SMPC components

Sensor/measuring technique	Material	Application	Remarks	References
Protractor tool	GFR Styrene-based SMPC	Space applications, not specified	The recovery angle was measured	19
Pressure sensors and protractor	CFR cyanate-based SMPC	Tip-loaded deployable truss	The recovery force under constrained condition and recovery angle under stress-free condition were measured	25
Force sensor, protractor, video camera and infrared thermal camera	CFR epoxy SMPC	Smart hinge	The recovery force, heat distribution, recovery angle and recovery speed were measured	27
Video-based image processing and thermal imaging camera	CFR SMPC prepreg	Model deployable solar panel array	The recovery angle and temperature distribution were measured	14
CMM and thermal imaging camera	CFR SMPC prepreg	Model deployable space habitat	The sample size and temperature distribution were measured	20
DIC	Epoxy based SMPs	Not specified	The surface strain was measured	21
DIC	CFR epoxy SMPC	Integrative hinge	The displacement and strain field were measured	26
FBG sensor	SMP epoxy and CFR prepreg	Aerospace actuator	The strain and temperature changes were measured	23
DOFS	CFR epoxy SMPC	Proposed for aerospace and biomedical applications	Spatially distributed dynamic temperature and strain fields were measured continually throughout the sample.	Current study

were determined. Consequently, the obtained experimental data were analyzed to quantify the shape recovery ratio, shape fixity ratio and shape recovery rate.

2 | MATERIALS AND METHODS

2.1 | Preparation of the DOFS embedded SMPC

To date, bisphenol A based SMPCs are extensively studied for aerospace applications³⁴ structural engineering applications⁹ and biomedical applications.³⁵ In this study, the SMP matrix material was synthesized by using bisphenol A epoxy resin and tetramine and jeffamine hardeners. Huntsman Australia supplied the bisphenol A epoxy resin and tetramine hardener (Aradur HY 951). Sigma Aldrich Australia supplied the Jeffamine (D230) hardener.

The chemical structures of the raw materials used to synthesize the SMP matrix are presented in Figure 1a. The Fourier-transform infrared spectrum of the bisphenol A epoxy-based CFR SMPC material is shown in Figure 1b. At room temperature, the flexural properties of the SMPC

material were investigated under the ASTM D790 testing standard and presented in Figure 1c. Accordingly, the flexural strength and the flexural modulus of the SMPC material were determined as 345 MPa and 8.33 GPa, respectively.

Bisphenol A diglycidyl ether resin and triethylenetetramine and poly(propylene glycol) bis(2-aminopropyl ether) hardeners were mixed to a stoichiometric ratio of 13.032:1.000:1.632, respectively. As a reinforcement material, two layers of carbon fiber were used. The 200 gsm, 0/90 woven, plain weave carbon fiber fabric was supplied by Colan Australia. The SMPC specimens were cast in a mold made by using two glass sheets and silicon sealant. The samples were first cured at room temperature for 24 h. Afterwards, the specimens were post cured at 100°C for 1.5 h and at 130°C for 1 h. Glass transition temperature of the prepared SMPC was 100°C (Tan Delta peak).

The DOFS embedded SMPC specimens were prepared by inserting a 125 μm single-mode optical fiber into the SMPC material. One end of the optical fiber was coupled to an FC/PC connector and the other end was kept free. Figure 2 illustrates the sensor layout all the way through the SMPC specimens. The DOFS was placed through an

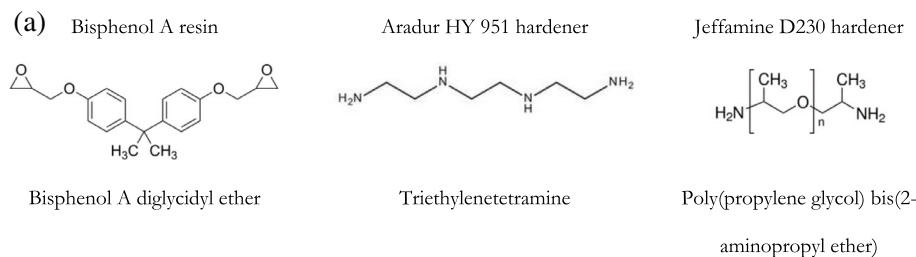
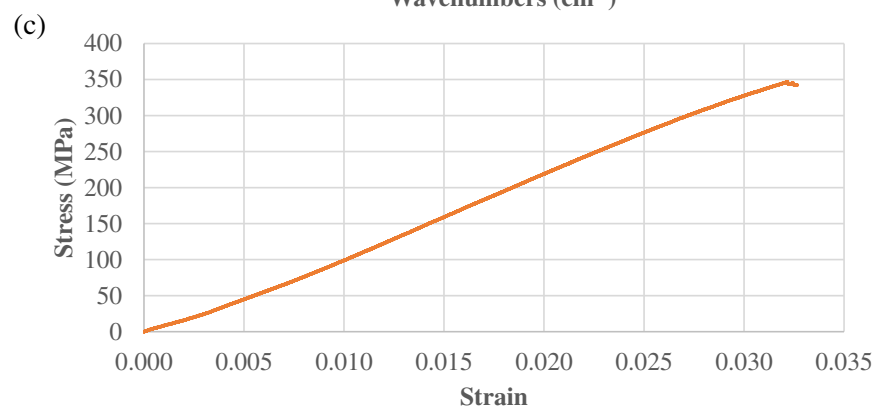
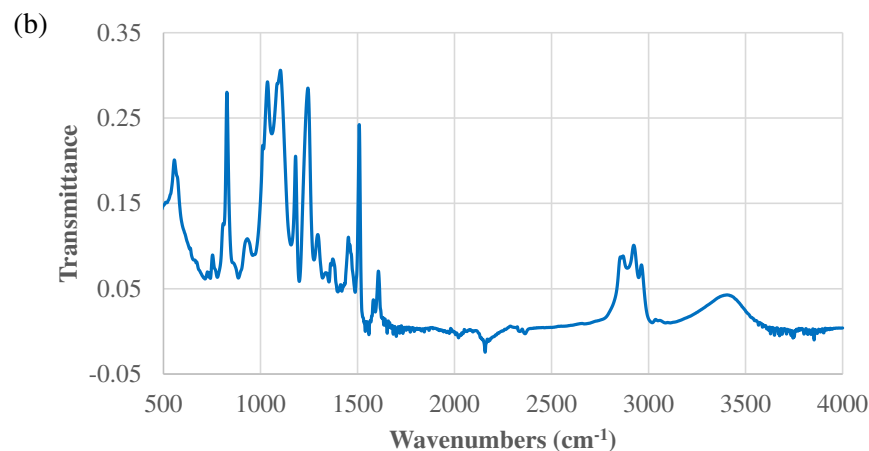


FIGURE 1 Details of the SMPC material (a) chemical structures of the raw materials used to synthesize the shape memory polymer (b) FTIR curve of the SMPC material (c) flexural stress-strain curve of the SMPC material [Color figure can be viewed at wileyonlinelibrary.com]



SMPC test specimen and a control specimen. The control specimen was used to compensate for the temperature effect during the shape recovery process, where strain decreases as temperature increases. Both test and control SMPC specimens were $200 \times 30 \times 2 \text{ mm}^3$ in size.

As illustrated in Figure 2, the optical fiber embedded into the SMPC specimens took letter “U” shaped paths. The bare optical fiber segments that were not embedded into the SMPC samples were protected with a low-density polyethylene (LDPE) tube. For the analysis, the sensor length embedded into the SMPC test specimen was considered as 0–400 mm. The sensor length of 0–200 mm provided the measurement along the first half of the embedded “U” shaped DOFS, and the sensor length of 200–400 mm provided the measurement along the second half in the SMPC test specimen. Therefore, the sensor lengths of 100 and 300 mm along the embedded sensor were considered as the bend location of the SMPC test specimen, where the point load was applied during the 3-point flexural test.

2.2 | Flexural shape memory test

The SMPC specimens were subjected to a three-point flexural shape memory test. To provide the necessary heat for the shape programming and recovery processes, SMPCs were placed inside an Instron temperature-controlled thermal chamber. The span between the roller supports was set to 100 mm. The external load necessary for shape programming was applied by using an MTS 10 kN, Insight electromechanical testing system. Figure 3 presents the experimental setup.

First, the enclosed thermal chamber was heated from room temperature (25°C) to a set temperature of 175°C (heat rate of $7.5^\circ\text{C}/\text{min}$) and kept isothermal for 10 min. Then the load was applied and the SMPC test specimen was flexed. The crosshead speed was set to 2 mm/min (downward). When the crosshead moved 20 mm, it was held fixed. Subsequently, the thermal chamber was kept open, allowing the SMPCs for natural cooling to a

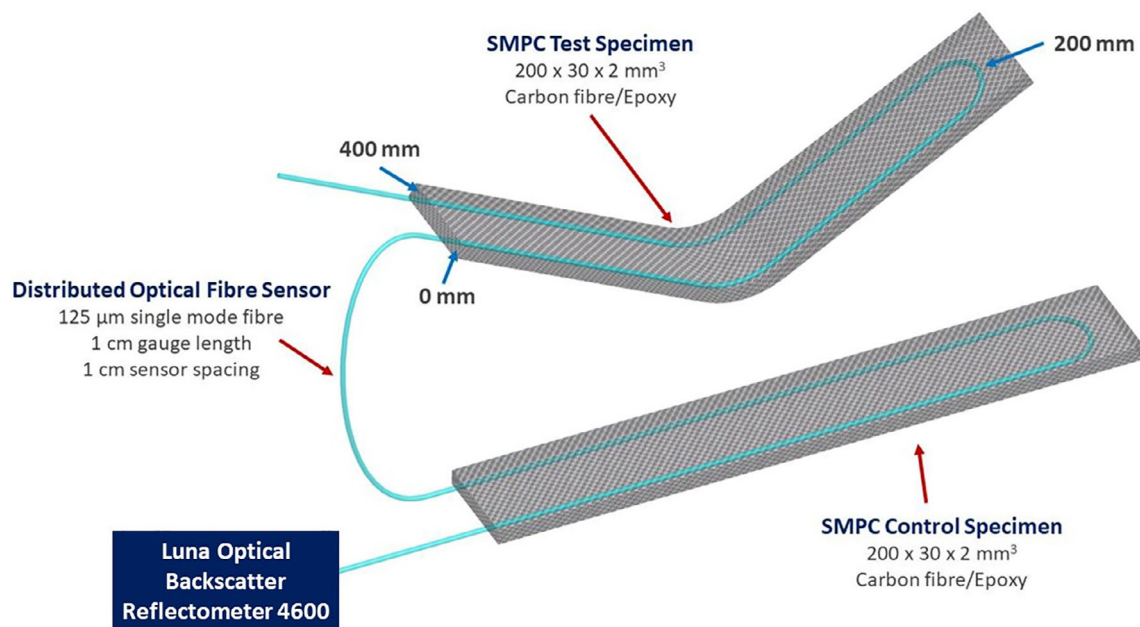


FIGURE 2 Layout of the distributed optical fiber sensor embedded into carbon fiber reinforced shape memory polymer composite (the SMPC test specimen illustrates the programmed temporary shape) [Color figure can be viewed at wileyonlinelibrary.com]

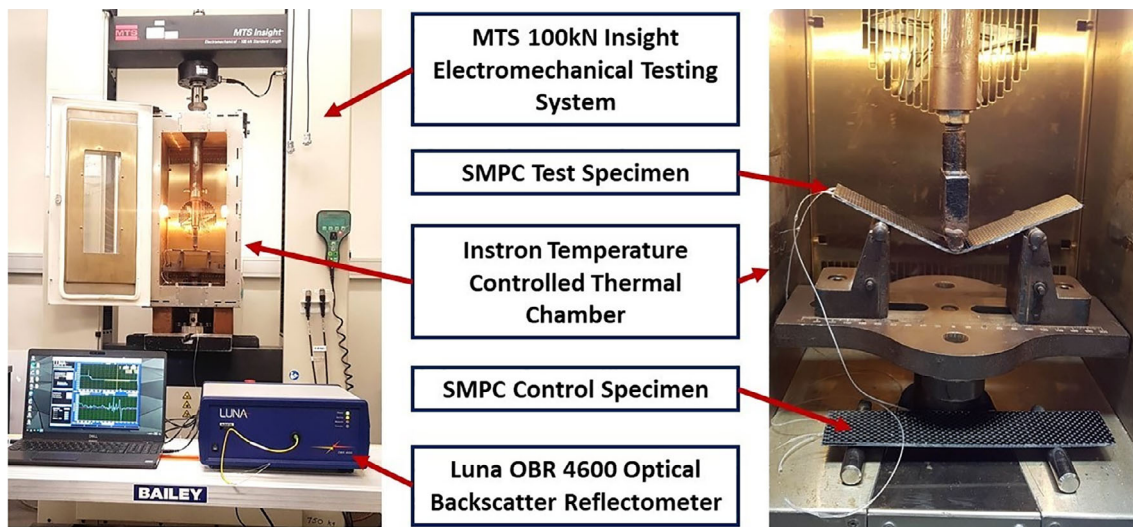


FIGURE 3 Experimental setup of the DOFS based real-time process monitoring under a three-point flexural shape memory process (the SMPC test specimen illustrates the programmed temporary shape) [Color figure can be viewed at wileyonlinelibrary.com]

TABLE 2 Measurements taken during the full thermomechanical cycle and the respective cycle time and the measuring location

Step	Cycle time	Shape memory process	OBR measurement	Location/specimen
1	0–30 min	Heat above T_g (temperature ramp, isostrain)	Temperature	Test specimen
2	30–40 min	Apply load for shape programming (strain ramp, isothermal)	Strain	Test specimen
3	40–55 min	Cool below T_g for shape fixing (temperature ramp, isostrain)	Temperature	Test specimen
4	55–60 min	Remove the external load (isothermal, isostrain)	Not measured	Not applicable
5	60–80 min	Heat above T_g for shape recovery (temperature ramp, dynamic strain)	Temperature Strain	Control specimen Test specimen

temperature below their T_g . After that, the crosshead was moved (upward) above the zero position and the thermal chamber was closed. Subsequently, the enclosed thermal chamber was heated up to a set temperature of 175°C (heat rate of 7.5°C/min) and kept isothermal for 5 min. In this article, the shape memory effect of the SMPC is presented by considering the five key steps described by Emmanuel et al.⁹ Accordingly, the full thermomechanical cycle was divided into five steps and detailed in Table 2.

For the duration of the entire shape memory process, the dynamic strain and temperature profiles were measured using a Luna OBR 4600 Optical Backscatter Reflectometer (OBR). The test parameters were set as; 1555.9–1577.2 nm scan range, 1.5 group index, 24 dB gain, 0.1 mm spatial resolution, 1 cm gauge length and 1 cm sensor spacing. Measurements were taken under the time domain and the measurement type was reflection mode. Table 2 describes the measurements obtained throughout the full thermomechanical cycle and the respective cycle time and the measuring location.

2.3 | Performance evaluation of the SMPC component

The strain and temperature profiles obtained from a DOFS were used to determine the real-time thermomechanical behavior of the SMPC material. Moreover, by considering the bend location as 100 mm sensor length, a full thermomechanical cycle was generated. The corresponding full thermomechanical cycle reflected the shape memory behavior of the respective bent location.

Fejős et al. devised equations to characterize the shape memory properties of an SMP material.³⁶ Accordingly, shape fixity ratio (R_f) and shape recovery ratio (R_r) were calculated by using Equations (1) and (2) respectively. Moreover, shape recovery rate (R_{rate}) was calculated by using Equation (3).

$$R_f = \frac{\varepsilon_u}{\varepsilon_m} \times 100\% \quad (1)$$

$$R_r = \frac{\varepsilon_m - \varepsilon_p}{\varepsilon_m - \varepsilon_0} \times 100\% \quad (2)$$

$$R_{rate} = \frac{\varepsilon_m - \varepsilon_p}{T_r - T_i} \quad (3)$$

where, ε_0 is the strain of the original shape; ε_m is the strain of the programmed temporary shape; ε_u is the strain of the fixed temporary shape; ε_p is the strain of the recovered shape; T_i is the time at which recovery begins; T_r is the time at which recovery is completed.

3 | RESULTS AND DISCUSSION

3.1 | Real-time thermomechanical behavior

Herein the real-time thermomechanical behavior of the carbon fiber reinforced SMPC sample was presented by considering the five process steps detailed in Table 2. The embedded DOFS used in this study provided continuous strain and temperature data along the embedded region in the SMPC test specimen and the control specimen. Figure 4 illustrates the temperature increase in the SMPC test specimen during step 1 of the thermomechanical cycle. In this study, a heating rate of 7.5°C/min was applied. Depending on the thickness of the sample, heat transfer into the material may be varied.³⁷ Accordingly, SMPCs with higher thickness require a lower heating rate. Herein the heating rate of 7.5°C/min was set by considering the preliminary shape memory experiments of the used SMPC material. However, the DOFS are capable of acquiring data in a pico-second with a sub-centimeter spatial resolution and for a kilometer level dynamic range.³⁸ Therefore, the DOSFs can be used to measure higher heating rates on demand. The temperature of the SMPC test samples showed a rapid increase during the first 7 min of heating. The overlapping shown by the curve associated with 3 min time might have been caused by the switching on and off behavior of the heating element to control the temperature in the thermal chamber. After the first 7 min, the temperature throughout the sample increased gradually and reached an average temperature of 166°C by the end of the heating process (step 1).

At the beginning of the heating process (0 min), the temperature throughout the SMPC specimen was almost

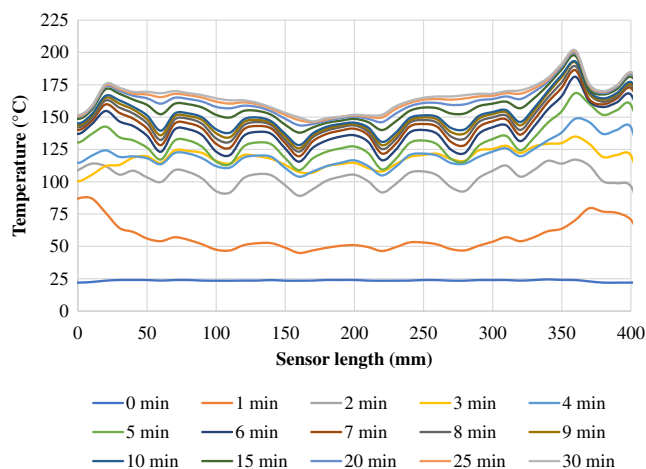


FIGURE 4 Temperature increase of the SMPC test sample during step 1 of the thermomechanical cycle [Color figure can be viewed at wileyonlinelibrary.com]

constant. However, during the temperature ramp, unanticipated temperature anomalies appeared. The reason for temperature anomalies might be the thermal stresses generated inside the SMPC during the heating process, which was not compensated for in this study. During the last 10 min of the heating process (step 1), the temperature inside the thermal chamber was kept constant. During this period the temperature anomalies disappeared because of the thermal stress relaxation.

Herein the bare optical fiber segments that were not embedded into the SMPC samples were protected with an LDPE tube. However, during the SMPC fabrication process, the LDPE tubes were slightly inserted into the SMPC specimens. Because of the protective cover and air gap between the DOFS and inner surface of the LDPE tube the temperature sensitivity of the DOFS might have been affected.³⁹ Filling a thermally conductive gel into the LDPE tube can enhance the temperature sensitivity of the protected areas of the DOFS.⁴⁰ However, in this study the LDPE embedded regions were located at the outer edges of the SMPC specimens that are insignificant in analyzing the shape memory effect of the test specimens. The temperature anomalies at the sensor lengths 20 and 360 mm might be due to the insertion of the LDPE protective tube into the SMPC specimen.

At a temperature below its T_g , the SMPC material was at its glassy phase and at a temperature above its T_g the SMPC material was at its rubbery phase. During step 2 of the thermomechanical cycle, the heated SMPC sample, which was at its rubbery phase was programmed under 3-point bending. Figure 5 shows the increase of load and deflection sensed by the electromechanical testing system, due to the flexure of the SMPC test sample. It was shown that the crosshead moved from 0 to 20 mm (downward direction) within 10 min. The linear deflection was caused by the crosshead speed that was set constant. The applied load increased from 0 to 4.6 N as the SMPC deformed. The increase in the load exhibited the elastic deformation of the SMPC, which was at the rubbery phase. The magnitude of the applied load (4.6 N) to program the temporary shape demonstrated the fixed strain (constrained), stress recovery performance of the SMPC.

It was noted that the shape programming by three-point flexural loading has produced a compression strain in the DOFS. It can be explained that the DOFS was mounted above the neutral axis and positioned close to the top surface of the SMPC test specimen. The strain variations of the SMPC test sample during step 2 of the thermomechanical cycle are presented in Figure 6. Originally the sensor lengths of 100 and 300 mm were set to coincide with the load applying axis (bend axis). During the shape programming process, the sensor length

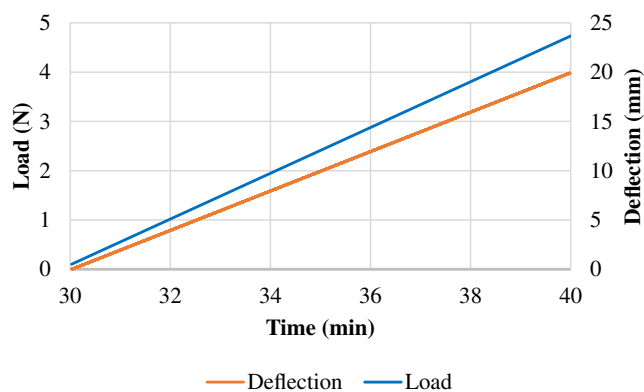


FIGURE 5 Load and deflection behavior of the SMPC test sample during step 2 of the thermomechanical cycle [Color figure can be viewed at wileyonlinelibrary.com]

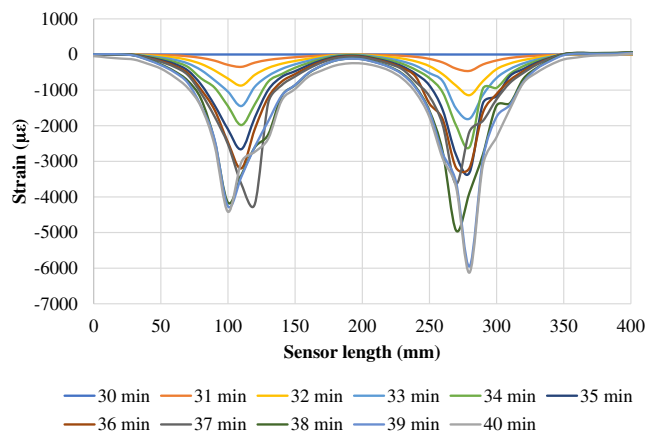


FIGURE 6 Strain variations of the SMPC test sample during step 2 of the thermomechanical cycle [Color figure can be viewed at wileyonlinelibrary.com]

associated with the peak strain was altered. At the end of the shape programming process (step 2), the DOFS readings demonstrated two strain peaks at 100 and 280 mm sensor locations. The extents of the peaked strains were -4420 and $-6125 \mu\epsilon$ at 100 and 280 mm sensor locations, respectively.

Originally, the 300 mm sensor length was considered as the bend location. However, after shape programming, the associated peak appeared at the 280 mm sensor length. Most likely the CFR SMPC laminates might have delaminated during the shape programming step. As a result, the portion of the peaked strain associated with 300 mm sensor length might have shifted by 20 mm. After the shape programming step, the extent of the strain at 280 mm sensor length ($-6125 \mu\epsilon$) demonstrated a higher compression strain of $1705 \mu\epsilon$ than the extent of the strain at 100 mm sensor length ($-4420 \mu\epsilon$). The difference in peaked strain values could also be attributed to

SMPC delamination. This observation revealed that the embedded DOFSs are capable of detecting not only the shape memory behavior but also the damages to the SMPC components during the memory processes. Therefore, the embedded DOFSs may also apply for structural health monitoring of the large SMPC structures throughout their lifetime. The DOFSs are well-suited for measuring large deformations of SMPs under flexural loading than axial loading. Moreover, CFR and GFR SMPCs have a limitation in large deformations under tensile and compression loading. Accordingly, DOFSs have the ability to measure tensile or compression deformations of fiber reinforced SMPCs until the failure occurs.

Subsequently, step 3 of the thermomechanical cycle utilized natural cooling to fix the temporary shape of the SMPC. As shown in Figure 7, the average temperature of the SMPC test specimen was reduced to 72°C (below T_g) at the end of the cooling process (step 3). However, the temperature profiles during the cooling step also showed unanticipated temperature anomalies. These temperature anomalies along the DOFS might have been caused by the uneven natural cooling that happened inside the thermal chamber. Additionally, the internal stresses caused by the thermal contraction resulting from the cooling might have affected the temperature measurements. The unusual temperature reductions associated with the sensor lengths 0–20 mm and 360–400 mm could be due to the insertion of the LDPE protective tube into the SMPC specimen. Afterwards, step 4 of the thermomechanical cycle removed the external load and closed the thermal chamber. During step 4, OBR measurements were not recorded.

During step 5 of the thermomechanical cycle, both strain and temperature of the SMPC test sample were varied simultaneously. However, the SMPC control sample was only subjected to temperature variations. Therefore, the effects of the corresponding temperature on the SMPC test sample was compensated by using the data acquired from the SMPC control sample. Figure 8 shows the temperature increase of the SMPC control sample during step 5 of the thermomechanical cycle. The temperature of the SMPC control samples showed a rapid increase during the first 7 min of step 5. Afterwards, the temperature in the sample increased only slightly.

Corresponding shape recovery behavior under step 5 of the thermomechanical cycle was studied by considering the strain variations of the SMPC test sample. Figure 9 presents the strain measurements obtained during the shape recovery process (step 5). During the recovery process, the strain data showed arbitrary anomalies. In addition, the sensor lengths associated with the strain peaks fluctuated slightly. It can be expected that the delamination that occurred during the shape

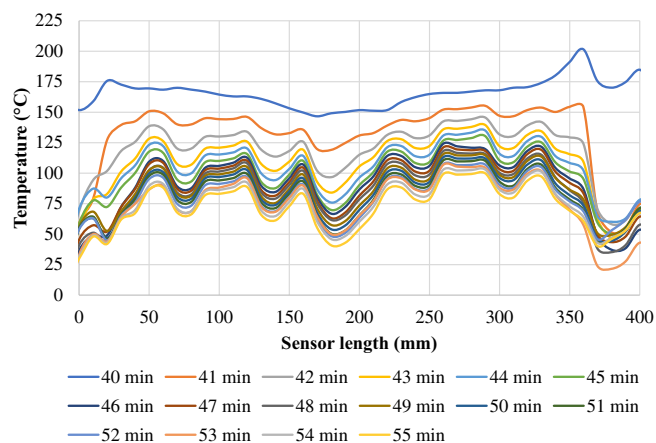


FIGURE 7 Temperature decrease of the SMPC test sample during step 3 of the thermomechanical cycle [Color figure can be viewed at wileyonlinelibrary.com]

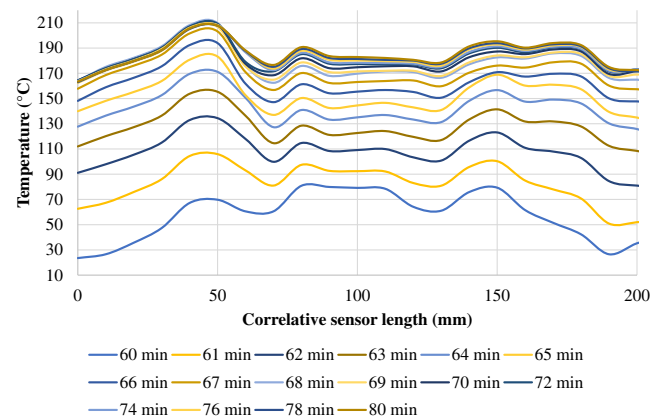


FIGURE 8 Temperature increase of the SMPC control sample during step 5 of the thermomechanical cycle [Color figure can be viewed at wileyonlinelibrary.com]

programming process (step 2), was further propagated during the shape recovery process (step 5), which might have caused the arbitrary strain variations. Interestingly, at the end of the recovery process shown in step 5, the average strain of the SMPC test sample reached $-3 \mu\epsilon$. The average strain of the original shape was considered to be $0 \mu\epsilon$. Therefore, it was revealed that the SMPC test sample almost reached the original shape after a full thermomechanical cycle.

3.2 | Shape memory characteristics

Figure 10 shows the behavior of the SMPC test specimen under a 3-point flexural shape memory process. The original shape of the SMPC test specimen was straight, where the bend angle was 180° . By considering the span

between the roller supports (100 mm) and the crosshead movement (20 mm) the bend angle of the programmed shape was calculated as 136° . Under shape fixing (step 3), the reversible crosslinks in the material microstructure have frozen to fix the material in its deformed shape. However, after the unloading phase (step 4), the fixed shape showed a spring-back effect. By using the Gwyddion open-source image processing software, it was determined that the bend angle shifted by $\sim 1.4^\circ$, because of the spring-back effect. Finally, at the recovery phase

(step 5), crosslinks released the stored strain energy and acquired the recovered shape. Image processing has not shown any difference between the original and recovered shapes.

Shape memory performances of polymer materials are generally quantified by using DMAs. When using a standard testing instrument such as DMA, it is impossible to test larger samples as the specimen size is usually around $60 \times 8 \times 5 \text{ mm}^3$. Furthermore, the deformation strains that can be applied during the programming stage are limited to a low strain range. Additionally, complex shape programming is impossible due to its fixture setup. However, customized programming procedures can overcome such drawbacks of standard testing apparatuses. The customized testing methods can be easily tailored to the requirements of the application. Moreover, larger samples can be tested effectively with required strain levels and complexity. Moreover, the widely used DMA experiments under single or dual cantilever methods provide thermomechanical measurements by considering the furnace temperature and the drive shaft movements.

Compared to the typical thermomechanical characterization methods such as DMA, the DOFS based measurements were able to provide thermal and mechanical characteristics continuously along the SMPC. Based on the application of these measurements, experimental data obtained from specific locations such as bend locations can be considered for the analysis. Herein, the thermomechanical measurements (temperature and strain) at 100 mm sensor location were

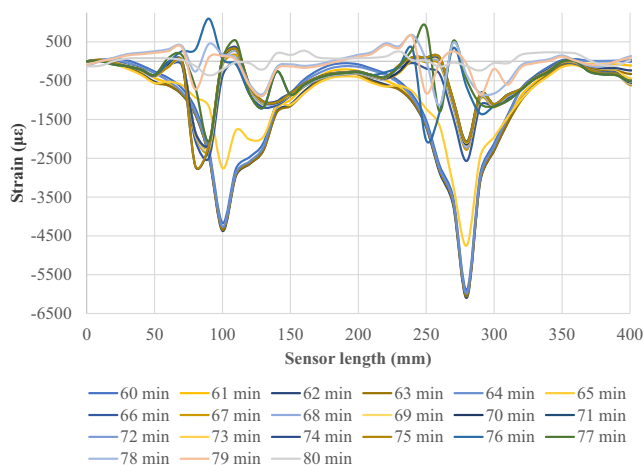


FIGURE 9 Strain variations of the SMPC test sample during step 5 of the thermomechanical cycle [Color figure can be viewed at wileyonlinelibrary.com]

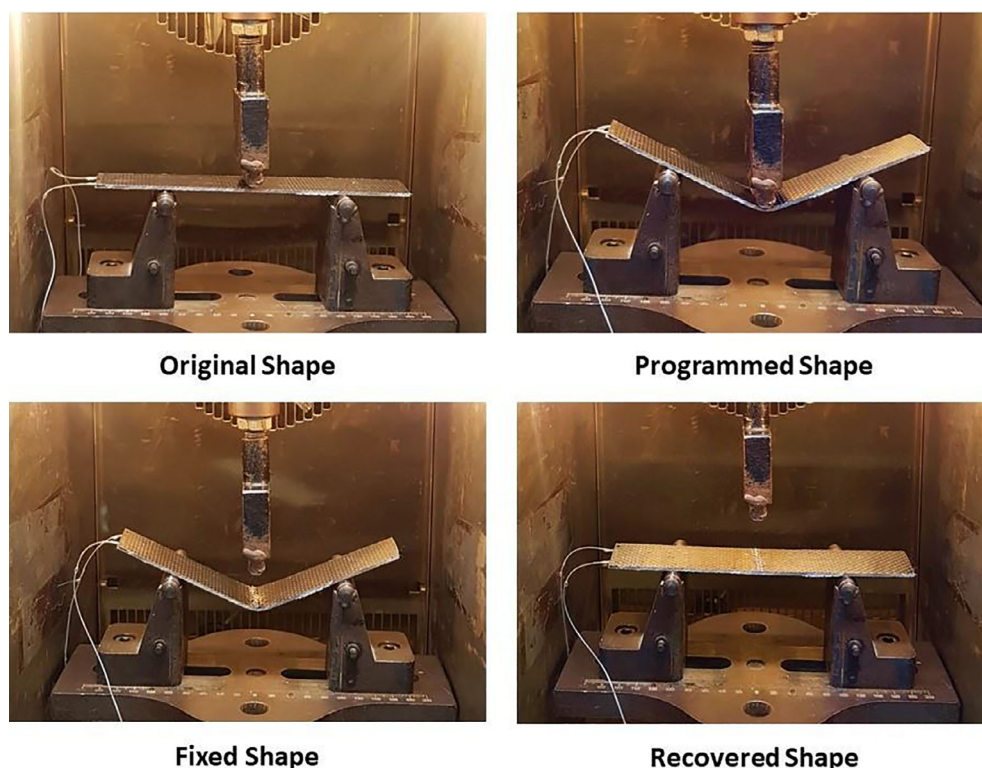


FIGURE 10 Shape memory behavior of the SMPC [Color figure can be viewed at wileyonlinelibrary.com]

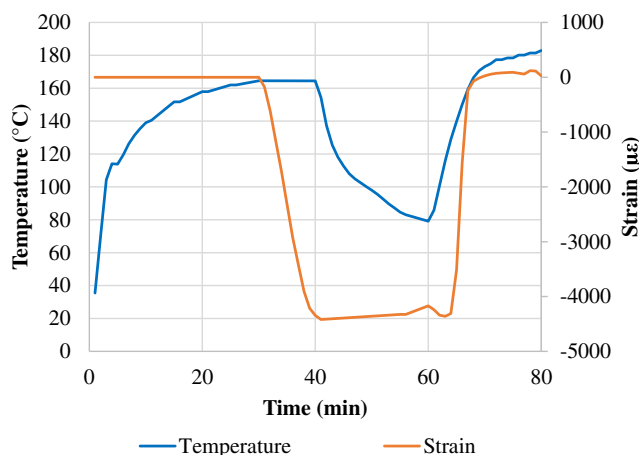


FIGURE 11 Full thermomechanical cycle at the bent location by considering the 100 mm sensor length [Color figure can be viewed at [wileyonlinelibrary.com](https://onlinelibrary.wiley.com)]

considered to characterize the SMPC. Only at the shape recovery phase (step 5), both the temperature and the strain were showing a variation. Therefore, the corresponding temperature data was compensated by using the data acquired from the SMPC control specimen.

Figure 11 shows the full thermomechanical cycle generated by considering the 100 mm sensor location of the SMPC specimen. According to Equations (1) and (2), shape fixity (R_f) and recovery (R_r) ratios of the SMPC were calculated as 94.5% and 99.9%, respectively. As per Equation (3), the shape recovery rate (R_{Rate}) at the 100 mm sensor location was determined as 10.61 $\mu\epsilon/s$.

4 | CONCLUSION

Critical analyses on real-time shape memory behavior and thermomechanical characteristics of SMP materials are essential to develop precise and reliable and engineering applications. The widely used test method for shape memory analysis, DMA, is only suitable for experiments with small scale test specimens during the material design and development phases. This study revealed the ability of an embedded DOFS to measure real-time temperature and strain variations throughout an SMPC, for the duration of the shape memory process. The DOFSs can be embedded into the large SMPC components during their manufacturing process. The proposed real-time measuring technique can be applied for large SMPC components such as booms, hinges, deployable solar panel arrays and deployable space habitats, which involves multiple locations of shape memory processes. The heat transferring behaviors and the shape memory characteristics such as shape fixity ratio, shape recovery ratio and

the shape recovery rate can be determined for any intended location over the embedded sensor length. Strategically, the customized testing method proposed herein can be easily tailored to the requirements of the intended application. Moreover, larger samples can be tested effectively with required strain levels and shape complexity. Further research is warranted to investigate the reliability of the proposed monitoring system in extreme operational environments.

ACKNOWLEDGMENTS

The corresponding author is indebted to the University of Southern Queensland, Australia for providing laboratory facilities and the materials used in this work. The authors are indebted to Dr. Barbara Harmes at the Language Centre of the University of Southern Queensland, Australia for the support provided on proofreading.

AUTHOR CONTRIBUTIONS

Madhubhashitha Herath: Conceptualization (lead); investigation (lead); methodology (lead); writing – original draft (lead). **Chris Emmanuel:** Investigation (equal); methodology (equal). **Janitha Jeewantha:** Investigation (equal); methodology (supporting); writing – original draft (supporting). **Jayantha Epaarachchi:** Conceptualization (supporting); methodology (equal); supervision (lead); writing – review and editing (equal). **Jinsong Leng:** Writing – review and editing (equal).

DATA AVAILABILITY STATEMENT

The data that support the findings of this study are available on request from the corresponding author. The data are not publicly available due to privacy or ethical restrictions.

ORCID

Madhubhashitha Herath  <https://orcid.org/0000-0002-6796-0802>

REFERENCES

- [1] M. Zare, M. P. Prabhakaran, N. Parvin, S. Ramakrishna, *Chem. Eng. J.* **2019**, 374, 706.
- [2] T. Liu, T. Zhou, Y. Yao, F. Zhang, L. Liu, Y. Liu, J. Leng, *Compos. Part A Appl. Sci. Manuf.* **2017**, 100, 20.
- [3] J. Leng, X. Lan, Y. Liu, S. Du, *Prog. Mater. Sci.* **2011**, 56(7), 1077.
- [4] Y. Chen, Z. Wang, Y. He, Y. J. Yoon, J. Jung, G. Zhang, Z. Lin, *Proc. Natl. Acad. Sci.* **2018**, 115(7), E1391.
- [5] W. Wang, Y. Liu, J. Leng, *Coord. Chem. Rev.* **2016**, 320-321, 38.
- [6] Y. Chen, Z. Wang, Y. W. Harn, S. Pan, Z. Li, S. Lin, J. Peng, G. Zhang, Z. Lin, *Angew. Chem. Int. Ed.* **2019**, 58(34), 11910.
- [7] W. Zhao, L. Liu, F. Zhang, J. Leng, Y. Liu, *Mater. Sci. Eng. C* **2019**, 97, 864.
- [8] M. Herath, J. Epaarachchi, Shape memory polymer composites and their smart structural applications. In *Composite*

- Materials* (Eds: I.-M. Low, Y. Dong), Elsevier, Amsterdam, Netherlands **2021**, p. 581.
- [9] K. D. C. Emmanuel, H. M. C. M. Herath, L. H. J. Jeewantha, J. A. Epaarachchi, T. Aravinthan, *Constr. Build. Mater.* **2021**, 303, 124442.
- [10] L. Wang, F. Zhang, Y. Liu, J. Leng, *Advan. Fiber Mater.* **2021**. <https://doi.org/10.1007/s42765-021-00073-z>.
- [11] R. Xiao, W. M. Huang, *Macromol. Biosci.* **2020**, 20(8), 2000108.
- [12] M. Behl, A. Lendlein, *Mater. Today* **2007**, 10(4), 20.
- [13] L. Dai, C. Tian, R. Xiao, *Int. J. Plast.* **2020**, 127, 102654.
- [14] H. M. C. M. Herath, J. A. Epaarachchi, M. M. Islam, W. al-Azzawi, J. Leng, F. Zhang, *Compos. Sci. Technol.* **2018**, 167, 206.
- [15] F. Li, Y. Liu, J. Leng, *Smart Mater. Struct.* **2019**, 28(10), 103003.
- [16] W. Zhao, L. Liu, J. Leng, Y. Liu, *Compos. Part B* **2019**, 179, 107455.
- [17] ASTM D5418 - Standard Test Method for Plastics: Dynamic Mechanical Properties: In Flexure (Dual Cantilever Beam). 2015, ASTM International.
- [18] M. Herath, J. Epaarachchi, M. Islam, C. Yan, F. Zhang, J. Leng, *J. Intell. Mater. Syst. Struct.* **2019**, 30(20), 1045389X19879998.
- [19] W. Al Azzawi, M. Herath, J. Epaarachchi, Modeling, analysis, and testing of viscoelastic properties of shape memory polymer composites and a brief review of their space engineering applications. In *Creep and Fatigue in Polymer Matrix Composites*, 2nd ed. (Ed: R. M. Guedes), Woodhead Publishing, Duxford, United Kingdom **2019**, p. 465.
- [20] H. M. C. M. Herath, J. A. Epaarachchi, M. M. Islam, J. Leng, *Engineer: J. Instit. Eng. Sri Lanka* **2019**, 52(1), 1.
- [21] K. Shahi, R. Boomurugan, R. Velmurugan, *Structures* **2020**, 29, 2082.
- [22] V. L. Le, V. T. Le, N. S. Goo, *J. Intell. Mater. Syst. Struct.* **2019**, 30(17), 2625.
- [23] S. Ameduri, M. Ciminello, A. Concilio, F. Quadrini, L. Santo, *Actuators* **2019**, 8(3), 51.
- [24] F. Quadrini, L. Santo, M. Ciminello, A. Concilio, R. Volponi, P. Spena, *AIP Conf. Proc.* **2016**, 1736(1), 020090.
- [25] F. Li, L. Liu, L. Du, Y. Liu, J. Leng, *Compos. Struct.* **2020**, 242, 112196.
- [26] T. Liu, L. Liu, M. Yu, Q. Li, C. Zeng, X. Lan, Y. Liu, J. Leng, *Compos. Struct.* **2018**, 206, 164.
- [27] Z. Liu, X. Lan, W. Bian, L. Liu, Q. Li, Y. Liu, J. Leng, *Compos. Part B* **2020**, 193, 108056.
- [28] X. Bao, L. Chen, *Sensors* **2012**, 12(7), 8601.
- [29] A. Masoudi, T. P. Newson, *Rev. Sci. Instrum.* **2016**, 87(1), 011501.
- [30] M. Herath, J. Epaarachchi, M. Islam, F. Zhang, J. Leng, L. Fang, C. Yan, G. D. Peng, W. Schade, *Smart Mater. Struct.* **2020**, 29(4), 047001.
- [31] M. Herath, J. Epaarachchi, M. Islam, L. Fang, J. Leng, *Eur. Polym. J.* **2020**, 136, 109912.
- [32] Herath, M., C. Emmanuel, J. Jeewantha and J. Epaarachchi. In-situ performance evaluation of large shape memory polymer components via distributed optical fibre sensors. 2021 10th Int. Conf. on Information and Automation for Sustainability (ICIAfS). **2021**.
- [33] L. H. J. Jeewantha, K. D. C. Emmanuel, H. M. C. M. Herath, J. A. Epaarachchi, M. M. Islam, J. Leng, *Materialia* **2021**, 21, 101264.
- [34] M. J. Jo, H. Choi, H. Jang, W. R. Yu, M. Park, Y. Kim, J. K. Park, J. H. Youk, *J. Polym. Res.* **2019**, 26(6), 129.
- [35] L. H. J. Jeewantha, K. D. C. Emmanuel, H. M. C. M. Herath, M. M. Islam, L. Fang, J. A. Epaarachchi, *Materialia* **2022**, 21, 101325.
- [36] M. Fejós, G. Romhány, J. Karger-Kocsis, *J. Reinf. Plast. Compos.* **2012**, 31(22), 1532.
- [37] Emmanuel, K.D.C., J. Jeewantha, M. Herath, J. Epaarachchi and T. Aravinthan. Effect of thickness on the shape memory properties of bisphenol A epoxy based shape memory polymer composites. ASME 2021 Conf. on Smart Materials, Adaptive Structures and Intelligent Systems. **2021**.
- [38] F. Esmailzadeh Noghani, S. Tofighi, N. Pishbin, A. R. Bahrampour, *Opt. Laser Technol.* **2019**, 115, 277.
- [39] E. K. G. Boateng, P. Schubel, R. Umer, *Sens. Actuat., A* **2019**, 287, 158.
- [40] P. A. Robertson, B. P. Ludden, A fibre optic distributed sensor system for condition monitoring of synthetic ropes. IEE Colloquium on Optical Techniques for Smart Structures and Structural Monitoring (Digest No. 1997/033). **1997**.

How to cite this article: M. Herath, C. Emmanuel, J. Jeewantha, J. Epaarachchi, J. Leng, *J. Appl. Polym. Sci.* **2022**, 139(22), e52247. <https://doi.org/10.1002/app.52247>